Design of a Welding Arm for Unibody Automobile Assembly

Joseph T. Wunderlich
Elizabethtown College
Computer Engineering Program
Elizabethtown, PA, USA

Abstract

Typical unibody assembly can require more than 5000 welds to connect the pressed-metal sheets that form the unibody. Robotic arms can be designed specifically for this task by permuting arm link-lengths and degrees-of-freedom (DOF) to find a set of feasible designs, with each design evaluated for joint-angle displacement, dexterity, simulated speed, and consumption of available redundancy. A heuristic search increases the probability of a design having the needed kinematic structure. Hyper-redundant designs of up to ten DOF can be created. The search often results in minimizing DOF. The path planning technique combines pseudoinverse velocity control with the concept of attractive-poles to allow maneuvering through complex enclosures while avoiding many obstacles simultaneously.

1 Introduction

A typical automobile unibody is shown in Fig. 1. and industrial robots performing unibody assembly are shown in Fig. 2. Most industrial arms are general-purpose, and welding tasks are often programmed by a technician using a *teach-pendant* to physically move the robot by hand into position while in *teach-mode*. However, the design of arms for specific tasks can easily be justified if the tasks are repeated millions of times per year for a fixed workspace. The average automobile unibody can require over 5000 separate welds.

The velocity of a robotic arm's end-effector is

$$\dot{\mathbf{x}}_e = \mathbf{J}_e \dot{\boldsymbol{\theta}} \qquad (1)$$

where $\mathbf{J}_e$ is the Jacobian matrix.

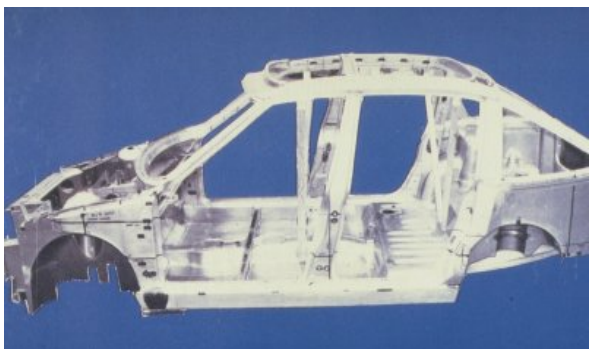

Figure 1. An automobile unibody [1].

Assuming $m>n$ where n is the arm's DOF and m is the dimension of the workspace, the general form of the least squares approximate solution to this underdetermined set of linear equations yields a joint-angle velocity vector:

$$\dot{\boldsymbol{\theta}} = \mathbf{J}_e^{\#}\dot{\mathbf{x}}_e + (\mathbf{I} - \mathbf{J}_e^{\#}\mathbf{J}_e)\dot{\Psi} \qquad (2)$$

where $\mathbf{I}$ is an identity matrix, $\dot{\Psi}$ is an arbitrary joint-velocity vector, $(\mathbf{I} - \mathbf{J}_e^{\#}\mathbf{J}_e)\dot{\Psi}$ is the projection of $\dot{\Psi}$ onto the null space of $\mathbf{J}_e$, and $\mathbf{J}_e^{\#}$ is the pseudoinverse:

$$\mathbf{J}_e^{\#} = \mathbf{J}_e^{T}(\mathbf{J}_e\mathbf{J}_e^{T})^{-1} \qquad (3)$$

Equation (2) represents the least-squares solution which minimizes the error norm:

$$\min \left\| \dot{\mathbf{x}}_e - \mathbf{J}_e\dot{\boldsymbol{\theta}} \right\| \qquad (4)$$

and focuses on the *exactness* of the solution [2]. The first term of (2) represents the minimum norm solution among all solutions provided by (2) by also satisfying

$$\min \left\| \dot{\boldsymbol{\theta}} \right\| \qquad (5)$$

which relates to the *feasibility* of implementing a solution since excessively large joint-angle velocities are not realizable [2].

In [3], $\dot{\Psi}$ in (2) is used to avoid obstacles by commanding joint-angle velocities to drive an arm's configuration toward a predetermined configuration previously proven to avoid a given obstacle. In [4], the null-space defined by the second term in (2) is used to define secondary and tertiary-priority tasks. In [5], this approach is modified to command a Cartesian velocity to repel the point on an arm closest to an obstacle directly away from the obstacle while attempting to maintain a *fixed* end-effector trajectory. However, in

Figure 2. Robots assembling unibody [1].

[6-11], it is noted that there are stability issues which must be addressed when using pseudoinverse velocity-control.

In [14], *local-attractors* pull the end-effector toward an attractive pole while joints are repelled from obstacles modelled as repulsive geometries. The end-effector trajectory is not fixed. In [15], hyper-redundant arms maneuver into enclosures by navigating through tunnels defined through the workspace. The arm is modelled as a continuous curve *threaded* through the tunnels and discretized into short equal-length link-lengths. This approach does not however consider unequal link-lengths and does not make use of much of the space within the enclosure. In [16], some general criteria for designing robotic arms are discussed including mechanical constructability and kinematic simplicity. In [17], the link-lengths of a two-link robotic arm are optimized for maximum acceleration and in [18] link-lengths of several commercial arms are evaluated using a dexterity measure (the condition number of the Jacobian). In [19], link-lengths are sized for specific tasks using random search algorithms.

2 Methodology

The design of a robotic arm to perform welding tasks in an automobile interior can be achieved by designing the arm for the most difficult task in the most constricted arm configuration. Fig. 3. shows the modelling of a workspace and an initial guess of an arm design. If the workspace is assumed to be approximately a cube, the design of a robot to perform a task in a two-dimensional square *slice* of the cube can define the most constricted work-area, requiring the most constricted kinematic configuration.

The initial guess of the arm's reach is that required for it to reach the furthest point in the cube. This design is then tested by commanding it to perform a welding task on the ceiling of the workspace as shown in Fig. 4. This is followed by a heuristic search process which permutes link-lengths and DOF to find a set of feasible designs for the given unibody interior. A final design is then chosen to meet a variety of performance criteria.

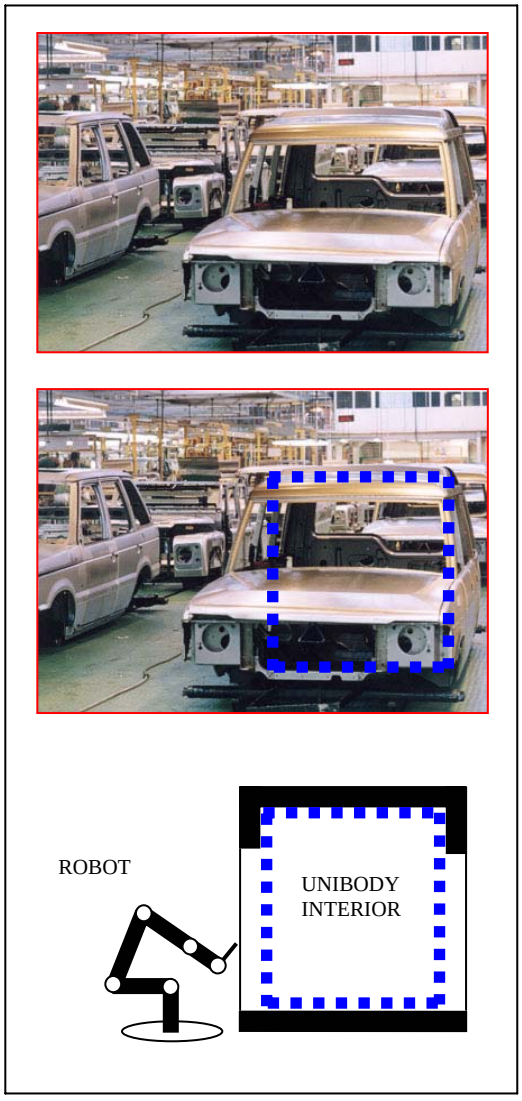

Figure 3. Robot workspace inside a unibody.

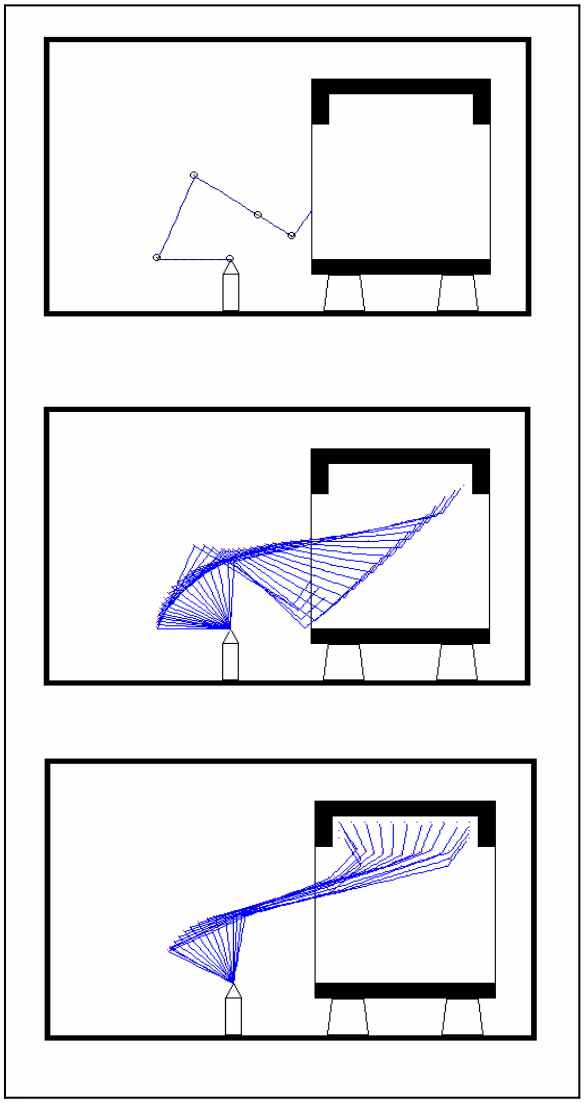

Figure 4. Initial arm design performing welding task inside unibody.

Many researchers have explored using fixed link-length, fixed DOF arms in constrained spaces [3]-[5], [14], [15], [20]-[22], and research has been conducted on optimizing link-lengths of non-redundant arms in unconstrained spaces [17], [18], [19], [23]. The method proposed here finds the needed link-lengths and DOF of redundant and non-redundant arms for a given unibody interior; and a path-planning technique is developed to test candidate designs.

Many performance measures have been proposed for evaluating arm trajectories. These include kinetic energy, joint torque [12], and many dexterity measures, [20], [21], [24]-[26]. The performance measures considered here are joint-angle displacement, dexterity, simulated speed, and a new measure: consumption of available redundancy (COAR). The control scheme is a variation of that used in [5] combined with a variation of that used in [14]. In [5] the $\dot{\Psi}$ in (2) is used to repel a point X_o on the arm away from obstacles by commanding a Cartesian velocity:

$$\dot{\mathbf{x}}_o = \mathbf{J}_o\dot{\boldsymbol{\theta}} \qquad (6)$$

where (*o*) designates the point on the arm closest to an obstacle (*obstacle-avoidance-point*). In [5], (2) is substituted into (6) to yield

$$\dot{\mathbf{x}}_o = \mathbf{J}_o\mathbf{J}_e{}^{\#}\dot{\mathbf{x}}_e + \mathbf{J}_o(\mathbf{I}-\mathbf{J}_e{}^{\#}\mathbf{J}_e)\dot{\Psi} \qquad (7)$$

where $\mathbf{J}_o\mathbf{J}_e{}^{\#}\dot{\mathbf{x}}_e$ is the Cartesian motion at the obstacle-avoidance-point to satisfy the end-effector velocity constraint. The second term of (7) represents the mapping of the $(\mathbf{I}-\mathbf{J}_e{}^{\#}\mathbf{J}_e)\dot{\Psi}$ null-space joint-velocity vector to a Cartesian vector at the obstacle-avoidance-point. The vector $\dot{\Psi}$ is found by re-writing (7) as

$$\dot{\mathbf{x}}_o - \mathbf{J}_o\mathbf{J}_e{}^{\#}\dot{\mathbf{x}}_e = \mathbf{J}_o(\mathbf{I}-\mathbf{J}_e{}^{\#}\mathbf{J}_e)\dot{\Psi} \qquad (8)$$

where $\dot{\mathbf{x}}_o - \mathbf{J}_o\mathbf{J}_e{}^{\#}\dot{\mathbf{x}}_e$ is the desired obstacle-avoidance-point Cartesian velocity:

$$\dot{\Lambda} = \dot{\mathbf{x}}_o - \mathbf{J}_o\mathbf{J}_e{}^{\#}\dot{\mathbf{x}}_e \qquad (10)$$

and $\mathbf{J}_o(\mathbf{I}-\mathbf{J}_e{}^{\#}\mathbf{J}_e)$ is the transformation of the orthogonal projection operator from the end-effector to the obstacle-avoidance-point:

$$\Gamma = \mathbf{J}_o(\mathbf{I}-\mathbf{J}_e{}^{\#}\mathbf{J}_e) \qquad (9)$$

Using (9) and (10), we can rewrite (8) as

$$\dot{\Lambda} = \Gamma\dot{\Psi} \qquad (11)$$

where the general form of the least squares $\dot{\Psi}$ solution is

$$\dot{\Psi} = \Gamma^{\#}\dot{\Lambda} + (\mathbf{I}-\Gamma^{\#}\Gamma)\dot{\beta} \qquad (12)$$

where **I** is an Identity matrix, $\dot{\beta}$ is an arbitrary vector, and $(\mathbf{I}-\Gamma^{\#}\Gamma)\dot{\beta}$ is the projection of $\dot{\beta}$ into the null space of Γ. This equation represents the least squares solution which minimizes the error norm:

$$\min\left\|\dot{\Lambda}-\Gamma\dot{\Psi}\right\| \qquad (13)$$

The first term of (12) represents the minimum-norm solution among all solutions provided by (12) by also satisfying:

$$\min\left\|\dot{\Psi}\right\| \qquad (14)$$

which has the effect of increasing the minimum obstacle distance [5]. Substituting (12) into (2) yields

$$\dot{\boldsymbol{\theta}} = \mathbf{J}_e{}^{\#}\dot{\mathbf{x}}_e + (\mathbf{I}-\mathbf{J}_e{}^{\#}\mathbf{J}_e)\Gamma^{\#}\dot{\Lambda} + (\mathbf{I}-\mathbf{J}_e{}^{\#}\mathbf{J}_e)\left[(\mathbf{I}-\Gamma^{\#}\Gamma)\dot{\beta}\right] \qquad (15)$$

In [5], it is shown that

$$\dot{\boldsymbol{\theta}} = \mathbf{J}_e{}^{\#}\dot{\mathbf{x}}_e + (\mathbf{I}-\mathbf{J}_e{}^{\#}\mathbf{J}_e)\left[\mathbf{J}_o(\mathbf{I}-\mathbf{J}_e{}^{\#}\mathbf{J}_e)\right]^{\#}(\dot{\mathbf{x}}_o - \mathbf{J}_o\mathbf{J}_e{}^{\#}\dot{\mathbf{x}}_e) \qquad (16)$$

and that the second term of (16) can be reduced to $\left[\mathbf{J}_o(\mathbf{I}-\mathbf{J}_e{}^{\#}\mathbf{J}_e)\right]^{\#}(\dot{\mathbf{x}}_o - \mathbf{J}_o\mathbf{J}_e{}^{\#}\dot{\mathbf{x}}_e)$ since the projection operator $(\mathbf{I}-\mathbf{J}_e{}^{\#}\mathbf{J}_e)$ is both hermetian and idempotent; therefore joint-angle velocities are governed by

$$\dot{\boldsymbol{\theta}} = \mathbf{J}_e{}^{\#}\dot{\mathbf{x}}_e + \left[\mathbf{J}_o(\mathbf{I}-\mathbf{J}_e{}^{\#}\mathbf{J}_e)\right]^{\#}(\dot{\mathbf{x}}_o - \mathbf{J}_o\mathbf{J}_e{}^{\#}\dot{\mathbf{x}}_e) \qquad (17)$$

by specifying a desired end-effector velocity $\dot{\mathbf{x}}_e$, and a desired obstacle-avoidance-point velocity $\dot{\Lambda} = \dot{\mathbf{x}}_o - \mathbf{J}_o\mathbf{J}_e{}^{\#}\dot{\mathbf{x}}_e$ through the selection of $\dot{\mathbf{x}}_o$.

The technique here allows many obstacles to be avoided simultaneously and is given by

$$\dot{\boldsymbol{\theta}} = \mathbf{J}_e^{\#}\dot{\mathbf{x}}_e + \sum_{i=1}^{N}\left[\left[\mathbf{J}_{o_i}(\mathbf{I}-\mathbf{J}_e^{\#}\mathbf{J}_e)\right]^{\#}\dot{\Lambda}\right] \qquad (18)$$

where $\dot{\Lambda}$ is commanded directly, and where N is the number of obstacle-avoidance-points; one fixed at each of the arm's joints (with the exception of the first two since they remain outside the enclosure). Up to eight obstacle-avoidance-points have been simulated on a 10-DOF robotic arm. Mid-link collisions with obstacles are avoided by setting minimum allowable distances

In [5], the use of multiple secondary-priority tasks is suggested for avoiding multiple obstacles by splitting the second term of (17) and scaling the new terms by relative distances to obstacles.

In (18), the summation terms are equally weighted. This requires the following additional measures to make the control scheme feasible:

- The end-effector is guided by *attractive poles* (similar to [14]) such that the trajectory can vary when available redundancy becomes diminished. (see Fig. 5)
- Available redundancy is conserved by repelling obstacle-avoidance-points in a direction related to end-effector trajectory.
- Obstacle-avoidance-points are repelled only within a designated area *close* to obstacles. This allows the arm to maneuver relatively unconstrained throughout a significant part of the enclosure. (see Fig. 5)
- Obstacle-avoidance-points are repelled with a velocity proportional to obstacle proximity. This provides smooth transitions for obstacle-avoidance-points into and out of the *repelling-fields*.

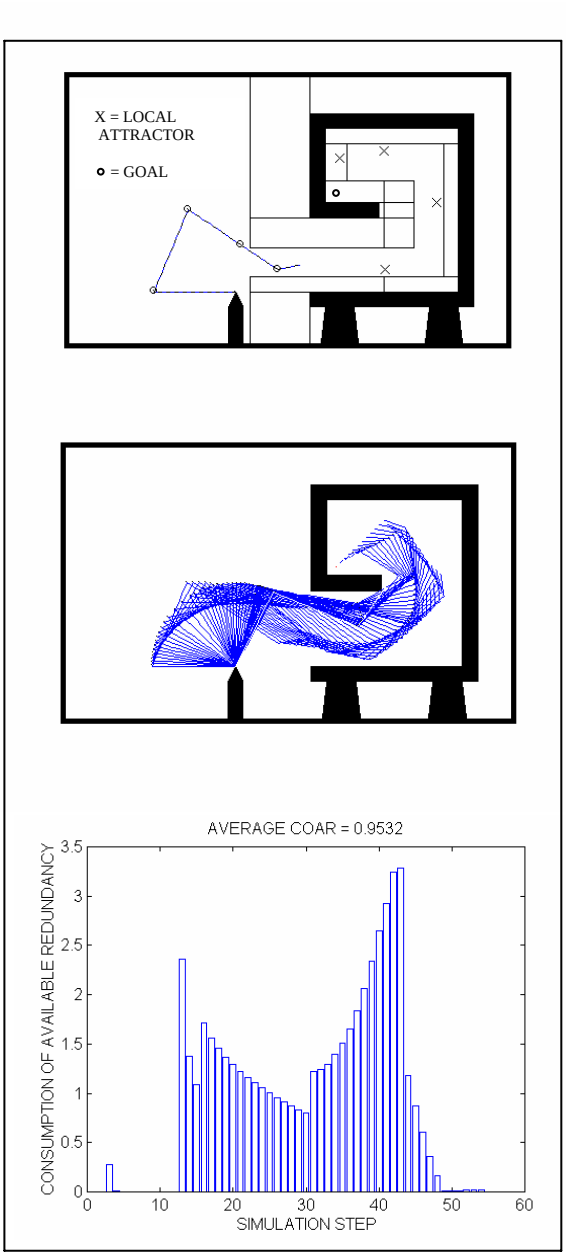

Figure 5. Consumption of available redundancy (COAR) over a highly constrained trajectory in a hypothetical enclosure.

2.1 Search for Feasable Designs

First an initial guess is made of arm kinematics; link-lengths and DOF are selected to allow the arm to reach the furthest point within the unibody while maintaining some length for maneuverability.

Repelling-velocity magnitudes for an initial design are found using repeated trial trajectories, and are not changed during a search. Once an initial design is found, one of several heuristics is used to search for new designs by changing link-lengths and testing each new design. Most searches are reduced by permuting link-lengths such that total arm length remains constant; and such that each new design doesn't *significantly* differ from its parent (e.g., by only changing two link-lengths each permutation). A search is continued until no new permutations are successful. An excess of links can be determined by setting the minimum link-length to zero; therefore the search can often result in the elimination of links (i.e., minimizing the required DOF).

The following measures aid in the final selection of an arm from a set of successful designs:

$\overline{COAR}_{02}$, R_{02}, $\hat{\overline{w}}_{12}$, and S_{02} are measures of consumption of available redundancy, joint-angle displacement, manipulability (dexterity), and simulation steps (simulated speed). Subscripts indicate when each is measured.

The consumption of available redundancy (COAR) is measured over each trajectory. Although the projection operator $(\mathbf{I}-\mathbf{J}_e^{\#}\mathbf{J}_e)$ in (2) maps any specified *n*-dimensional joint-velocity vector $\dot{\Psi}$ to a vector orthogonal to the *m*-dimensional Cartesian end-effector velocity manifold, the use of (17) or (18) can not guarantee a fixed end-effector trajectory if the available redundancy is exceeded. The *Consumption of Available Redundancy (COAR)* gives an indication of how the available redundancy is used over a trajectory:

$$COAR = \left[\frac{\left\|(\mathbf{I}-\mathbf{J}_e^{\#}\mathbf{J}_e)\dot{\Psi}\right\|}{\left\|\mathbf{J}_e^{\#}\dot{\mathbf{x}}_e\right\|}\right] = \left[\frac{\left\|\left[\mathbf{J}_o(\mathbf{I}-\mathbf{J}_e^{\#}\mathbf{J}_e)\right]^{\#}(\dot{\mathbf{x}}_o-\mathbf{J}_o\mathbf{J}_e^{\#}\dot{\mathbf{x}}_e)\right\|}{\left\|\mathbf{J}_e^{\#}\dot{\mathbf{x}}_e\right\|}\right] \quad (19)$$

Dividing by $\left\|\mathbf{J}_e^{\#}\dot{\mathbf{x}}_e\right\|$ in (19) normalizes the measure. The COAR varies significantly over a trajectory when the $d\theta_i$'s at each simulation step vary significantly due to obstacle avoidance. In contrast, $d\theta_i$'s for a minimum norm solution (i.e., no obstacle avoidance) vary the least and therefore result in the smallest Euclidean norm, and zero COAR. For multiple obstacle-avoidance-points, the consumption of available redundancy is

$$COAR = \left[\frac{\left\|(\mathbf{I}-\mathbf{J}_e^{\#}\mathbf{J}_e)\dot{\Psi}\right\|}{\left\|\mathbf{J}_e^{\#}\dot{\mathbf{x}}_e\right\|}\right] = \left[\frac{\left\|\sum_{i=1}^{N}\left[\mathbf{J}_{o_i}(\mathbf{I}-\mathbf{J}_e^{\#}\mathbf{J}_e)\right]^{\#}(\dot{\mathbf{x}}_{o_i}-\mathbf{J}_{o_i}\mathbf{J}_e^{\#}\dot{\mathbf{x}}_e)\right\|}{\left\|\mathbf{J}_e^{\#}\dot{\mathbf{x}}_e\right\|}\right] \quad (20)$$

and the average consumption of available redundancy over a trajectory is

$$\overline{COAR}_{02} = \left[\frac{\int_{t0}^{t_2}(COAR)dt}{t_2-t_0}\right] \quad (21)$$

and is lowest when the arm can avoid deep penetration into the repelling-fields and maneuver in the *free-space* in-between (see Fig. 5). t_0 is the initial time the end-effector enters the enclosure. t_1 is when the arm begins a welding task and t_2 is when it completes it.

Joint-angle displacement is measured by:

$$R_{02} = \int_{t0}^{t_2} \left(\sum_{i=1}^{DOF} \left| \Delta\theta_i(t) \right| \right) dt \qquad (22)$$

where $\Delta\theta_i(t)$ is the change in joint-angle θ_i during a simulation step. R_{02} is related to the mechanical work required to maneuver through the enclosure.

Although many dexterity measures have been proposed [20], [21], [24]-[26], one of the most referenced is the *measure of manipulability* developed in [20]:

$$w = \sqrt{\det(\mathbf{J}\mathbf{J}^T)} \qquad (23)$$

which gives an indication of how far an arm configuration is from a singularity (i.e., w = 0 at a singularity). Here, manipulability is measured while performing a welding task and an average manipulability is defined for all configurations along this trajectory as

$$\overline{w}_{12} = \left[\frac{\int_{t1}^{t_2} \left(\sqrt{\det(\mathbf{J}\mathbf{J}^T)} \right) dt}{t_2 - t_1} \right] \qquad (24)$$

and since manipulability is a function of link-lengths, the measure is normalized:

$$\hat{\overline{w}}_{12} = \left[\frac{\overline{w}_{12}}{\hat{w}_{\max}} \right] \qquad (25)$$

termed here the *normalized average manipulability*, ranging from 0 to 1. The maximum manipulability $\hat{w}_{\max}$ for each design corresponds to an optimal configuration $\boldsymbol{\theta}_{\hat{w}_{\max}}$ found at

$$\nabla_{\boldsymbol{\theta}} w(\boldsymbol{\theta})\Big|_{\boldsymbol{\theta}=\boldsymbol{\theta}_{\hat{w}_{\max}}} = 0 \qquad (26)$$

With a good initial guess, $\boldsymbol{\theta}_{\hat{w}_{\max}}$ is found for each design using only a few gradient steps with the search algorithm:

$$\boldsymbol{\theta}_t = \boldsymbol{\theta}_{t-1} + \eta \left[\nabla w(\theta_{t-1}) \right] \qquad (27)$$

where η is the step size selected for fast convergence without overshoot or divergent oscillation [27], [28], [29].

Simulated speed (S_{02}) is simply a measure of the number of simulation steps in a trajectory.

3 Results

Using a search that only changes link lengths by 10cm., two links at a time, results in 2189 new welding-arm designs from the original (90 120 95 50 40)cm. 5-DOF arm shown in Fig.4. This includes 104 4-DOF designs. Another search; one designed specifically to minimize DOF, quickly yields 15 4-DOF designs (and 41 5-DOF designs). One of these is shown in Fig. 6. This design also demonstrated some of the best manipulability, COAR, simulated speed, and joint angle displacement.

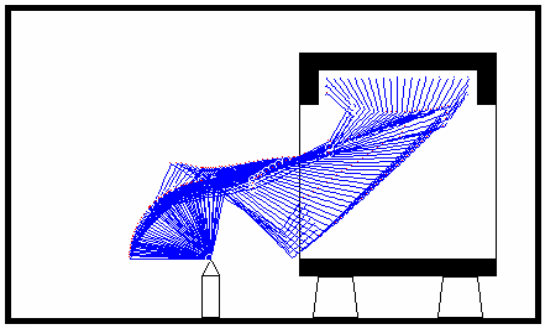

Figure 6. 4-DOF unibody welding-arm design found from applying a heuristic search to the original 5-DOF design of Fig. 4.

The robustness of the path-planning scheme is demonstrated in Fig. 7. where a 10-DOF hyper-redundant arm design is shown reaching all of a workspace deep with in a hypothetical interior.

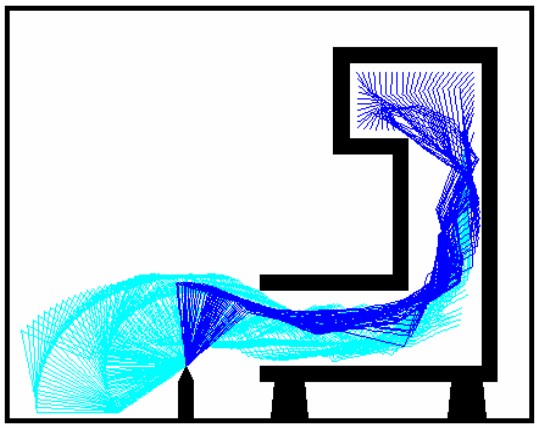

Figure 7. 10-DOF design reaching all of a target-workspace deep within a hypothetical interior.

4 Conclusions

Robotic arms to perform welding tasks inside unibody interiors can be designed by using heuristics to permute link-lengths and minimize DOF. The design process can be further refined by comparing feasible designs for maximum simulated speed and dexterity, and minimum joint-angle displacement and consumption of available redundancy over test-trajectories. A pseudoinverse path-planning technique is developed to allow maneuvering through a unibody interior by only repelling the arm within close proximity to obstacles, and at simulated velocities

proportional to proximity. Although using null space for path-planning can often cause stability problems, several measures are taken which allow the arm designs a degree of robustness in this environment; and more importantly, these designs can be used with other control schemes since they have been proven capable of operating within the given unibody.

References

[1] *TWI Image Library*, TWI World Center for Materials Joining Technology, 2004 [online]. Available: www.twi.co.uk/j32k/unprotected/band_1/imglb013.html

[2] Y. Nakamura and H. Hanafusa, "Singularity low-sensitive motion resolution of articulated robot arms," *Trans. Society of Instrument and Control Engineers*, vol. 20, no. 5, pp. 453-459, 1984.

[3] H. Hanafusa, T. Yoshikawa**,** and Y. Nakamura, "Analysis and control of articulated robot arms with redundancy," in *Proc. IFAC Control Science and Technology 8th Triennial World Congress*, 1981.

[4] Y. Nakamura, H. Hanafusa, and T. Yoshikawa, "Task-priority based redundancy control of robot manipulators," *Int. J. Robotics Res.*, vol. 6, no. 2, pp. 3-15, 1987.

[5] A. A. Maciejewski and C. A. Klein, "Obstacle avoidance for kinematically redundant manipulators in dynamic varying environments," *Int. J. Robotics Res.*, vol. 4, no. 3, pp. 109-117, 1985.

[6] B. Nemac, L. Zlajpah, and D. Omrcen. "Stability of null space control algorithms," in *Proc. RAAD'03 Int. Workshop on Robotics*, Alpe-Adria-Danube Region, Cassino, May, 2003.

[7] J. D. English and A. A. Maciejewski. "On the implimentation of velocity control for kinematically redundant manipulators," *IEEE Trans. Syst., Man, and Cybern.*, vol.30, no..3, May, 2000.

[8] B. Nemec and L. Zlajpah. "Experiments with force control of redundant robots in unstructured environment using minimal null-space formulation," *Journal of Advanced Computational Intelligence*, 5(5), pp.263 – 268, 2001.

[9] B. Nemec and L. Zlajpah. "Null velocity control with dinamically consistent pseudoinverse," *Robotica*, 18, pp. 513 – 518, 2000.

[10] J. T. Wunderlich and C. G. Boncelet, "Local optimization of redundant manipulator kinematics within constrained workspaces," in *Proc. of IEEE Int'l Conf. on Robotics and Automation*, Minneapolis, MN, 1996.

[11] J. T. Wunderlich, "Optimal kinematic design of redundant and hyper-redundant manipulators for constrained workspaces," Ph.D. dissertation, University of Delaware, May 1996.

[12] K. Kazerounian and Z. Wang, "Global versus local optimization in redundancy resolution of robotic manipulators," *Int. J. Robotics Res.*, vol. 7, no. 5, pp. 3-12, 1988.

[13] D. P. Martin, J. Baillieul, and J. M. Hollerbach, "Resolution of kinematic redundancy using optimization techniques," *IEEE Trans. Robotics and Automation*, vol. 5, no. 4, pp. 529-533, 1989.

[14] O. Khatib, "Real-time obstacle avoidance for manipulators and mobile robots," in *Proc. IEEE Int.Conf. on Robotics and Automation*, 1985.

[15] G. S. Chirikjian, J. W. Burdick, "An obstacle avoidance algorithm for hyper-redundant manipulators," in *Proc. IEEE Int. Conf. on Robotics and Automation*, 1990.

[16] J. M. Hollerbach, "Optimum kinematic design for a seven degree of freedom manipulator," in *Proc. Int. Symp.of Robotics Res.,"* 1988.

[17] Z. Shiller and S. Sundar, "Design of robotic manipulators for optimal dynamic performance," in *Proc. IEEE Int. Conf. on Robotics and Automation*, 1991.

[18] R. V. Mayorga, B. Ressa, and A. K. C. Wong, "A kinematic criterion for the design optimization of robot manipulators," in *Proc. IEEE Int. Conf. on Robotics and Automation*,1991.

[19] C. J. J. Paredis and P. K. Khosia, "Kinematic design of serial link manipulators from task specifications," *Int. J. Robotics Res.*, vol. 12, no. 3, pp. 274-287, 1993.

[20] T. Yoshikawa, "Analysis and control of robot manipulators with redundancy," in *Robotics Research*, eds. M. Brady and R. Paul, Cambridge, MA: MIT Press, 1984.

[21] C. A. Klein, "Use of redundancy in the design of robotic systems," in *Proc.2nd Int. Symp. On Robotics Res.*,1985.

[22] G. S. Chirikjian and J. W. Burdick, "Parallel Formulation of the inverse kinematics of modular hyper-redundant manipulators," in *Proc. IEEE Int. Conf. on Robotics and Automation*,1991.

[23] Y. Nakamura, *"Advanced robotics: redundancy and automation."* Reading, MA: Addison-Wesley, 1991.

[24] T. Yoshikawa, "Manipulablity of robotic mechanisms," *Int. J. Robotics Res.*, vol. 4, no. 2, pp. 3-9, 1984.

[25] F. C. Park and R. W. Brockett, "Kinematic dexterity of robotic mechanisms," *Int. J. Robotics Res.*, vol. 13, no. 1, pp. 1-15, 1994.

[26] K. L. Doty, C. Melchiorri, E. M. Schwartz, and C. Bonivento, "Robot manipulability," *IEEE Trans. Robotics and Automation*, vol. 11, no. 3, pp. 462-468, 1995.

[27] E. Kreyszig, *"Advanced Engineering Mathematics."* 6th ed. New York: John Wiley and Sons, 1988.

[28] R. L. Burden and J. D. Faires, *"Numerical Analysis."* 4th ed. Boston: PWS-Kent, 1989.

[29] J. Hertz, A. Krogh, and R. G. Palmer, *"Introduction to the theory of Neural Computation."* Redwood City, CA: Addison-Wesley, 1991.

JOSEPH T. WUNDERLICH

Dr. Wunderlich is the primary Computer Engineering Program Coordinator for Elizabethtown College. Previously, he worked for Purdue University as an Assistant Professor and for IBM as a researcher and hardware development engineer. Dr. Wunderlich received his Ph.D. in Electrical and Computer Engineering from the University of Delaware, his Masters in Engineering Science from the Pennsylvania State University, and his B.S. in Engineering from the University of Texas at Austin. He also has experience as an industrial automation consultant.